Computers, Materials & Continua

Tech Science Press

Doi:10.32604/cmc.2025.072776

ARTICLE

Energy Efficiency and Total Mission Completion Time Tradeoff in Multiple UAVs-Mounted IRS-Assisted Data Collection System

Hong Zhao, Hongbin Chen*, Zhihui Guo, Ling Zhan and Shichao Li

School of Information and Communication, Guilin University of Electronic Technology, Guilin, 541004, China

*Corresponding Author: Hongbin Chen. Email: chbscut@guet.edu.cn

Received: 03 September 2025; Accepted: 15 October 2025; Published: 09 December 2025

ABSTRACT: UAV-mounted intelligent reflecting surface (IRS) helps address the line-of-sight (LoS) blockage between sensor nodes (SNs) and the fusion center (FC) in Internet of Things (IoT). This paper considers an IoT assisted by multiple UAVs-mounted IRS (U-IRS), where the data from ground SNs are transmitted to the FC. In practice, energy efficiency (EE) and mission completion time are crucial metrics for evaluating system performance and operational costs. Recognizing their importance during data collection, we formulate a multi-objective optimization problem to maximize EE and minimize total mission completion time simultaneously. To characterize this tradeoff while considering optimization objective consistency, we construct an optimization problem that minimizes the weighted sum of the total mission completion time and the reciprocal of EE. Due to the non-convex nature of the formulated problem, obtaining optimal solutions is generally challenging. To tackle this issue, we decompose it into three sub-problems: UAV-SN association, number of reflecting elements allocation, and UAV trajectory optimization. An iterative algorithm combining genetic algorithm, CS-BJ algorithm, and successive convex approximation technique is proposed to solve these sub-problems. Simulation results demonstrate that when the transmitted data amount is 10 and 30 Mbits, compared to the static collection benchmark (the UAV hovers directly above each SN), the EE of the proposed method improves by more than 10.4% and 5.2%, while the total mission completion time is reduced by more than 5.4% and 3.3%, respectively.

KEYWORDS: Unmanned aerial vehicle; intelligent reflecting surface; energy efficiency; total mission completion time; optimization

1 Introduction

Sensors can be deployed in farmlands to collect environmental data such as soil moisture, air temperature, and wind speed, laying the foundation for Internet of Things (IoT) in precision agriculture [1]. However, limited energy storage restricts their operational lifespan. If sensor-collected data cannot be transmitted to the fusion center (FC) promptly, the finite memory capacity of sensors may lead to data overwriting. Furthermore, obstacles between sensors and the FC can result in incomplete data transmission due to the lack of a direct line-of-sight (LoS) path.

To address these issues, unmanned aerial vehicles (UAVs) have been leveraged as mobile base stations (BSs), relays, or data collectors [2]. Their high mobility and flexible deployment enable them to establish effective communication links, effectively mitigating non-line-of-sight (NLoS) problems. Nevertheless, UAVs are constrained by battery power, limiting their flight range and operational duration. This makes optimizing UAV trajectories crucial for energy-efficient data collection, especially when sensor nodes (SNs)

are widely dispersed [3]. For tasks beyond the capability of a single UAV, collaborative multi-UAV systems are deployed [4], often by partitioning SNs among UAVs for full coverage [5]. Research in multi-UAV systems has focused on various objectives, including minimizing energy consumption [6], reducing the maximum task completion time [7], lowering costs [8], and enhancing data collection rates [9]. Further studies explore tradeoffs between performance metrics, such as balancing computation capacity and energy consumption [10] or optimizing energy usage vs. task completion time [11].

As another way to improve channel quality, intelligent reflecting surface (IRS) manipulates incident signal propagation [12], enabling communication between SNs and FC without deploying costly mobile base stations (BSs) or relays, thereby enhancing energy and spectral efficiency (EE and SE) for reliable system performance. Conventional IRS is installed on building surfaces [13], offering ease of installation but limited coverage and mobility. To address this, researchers propose integrating IRS with UAVs. UAV-mounted IRS (U-IRS) [14] delivers superior flexibility, link quality, and coverage for SNs. In such U-IRS-assisted IoT, SNs transmit signals to the FC via U-IRS, effectively bypassing NLoS channel limitations.

1.1 Related Work

As a transformative technology, U-IRS significantly enhances the performance of IoT. Existing studies broadly fall into single-U-IRS and multi-U-IRS-assisted IoT, as summarized below.

1.1.1 Single-U-IRS-Assisted IoT

Researchers primarily focus on enhancing capacity/achievable rate, reducing energy consumption, and improving EE. Notably, Ref. [14] pioneered the concept of U-IRS and demonstrated its advantage over terrestrial IRS in terms of average data rate and LoS probability, laying the foundation for subsequent studies. Subsequent studies typically involve the joint optimization of parameters such as SN transmit power, UAV trajectory, IRS phase shifts, and the number of reflecting elements (NoRE) to maximize the sum rate [15–17] or the minimum data rate [18]. Other works have extended these optimizations to maximize secrecy rate [19–21] or to design energy-aware trajectories [22–24]. Metrics like EE, defined as the total information bits per propulsion energy, have been quantified to explore rate-energy tradeoff [25], with further investigations into solar-powered U-IRS for EE maximization [26] and applications in maritime communications [27]. A max-min optimization framework for covert throughput and propulsion efficiency was proposed in [28].

However, a common shortcoming of these single-U-IRS studies is their inherent limitation in coverage and task capacity. The performance of a single U-IRS is bounded by the UAV's limited flight endurance and range. Consequently, they are unsuitable for large-scale IoT deployments where SNs are widely dispersed, creating a clear motivation for employing multiple collaborative U-IRSs.

1.1.2 Multi-UAV IRS-Assisted IoT

For complex tasks exceeding single-UAV capabilities, multi-U-IRS collaboration is essential. However, research in this area remains sparse. Existing works have jointly optimized UAV placement, BS beamforming, and IRS passive beamforming to maximize the weighted sum rate [29], minimized UAV energy consumption in mobile-edge computing networks [30], derived outage probability for non-orthogonal multiple access (NOMA) systems [31], and minimized the maximum task offloading time by optimizing UAV positions [32].

1.1.3 Challenges in Existing Studies

Based on the above review, we identify the following specific gaps in the current literature on multi-U-IRS-assisted IoT:

i) **Impact of NoRE:** While parameters like trajectory and phase shifts are extensively optimized, with less consideration given to the impact of NoRE in the IRS. Although studies like [22,23] that analyze NoRE assume identical channel characteristics for all reflecting elements, resulting in low accuracy in the optimal NoRE.

ii) **Optimization of total task completion time:** In practical scenarios like smart agriculture, where frequent data collection is needed, minimizing the total mission completion time is vital for long-term cost efficiency. The number of UAVs, the energy provided to UAVs, and the flight trajectories of UAVs all affect the total mission completion time, which is related to costs. While prior multi-UAV research has focused on minimizing the maximum completion time (critical for time-sensitive applications like disaster relief or emergency communications), e.g., [7]. This metric does not guarantee a minimal total completion time. For instance, optimizing two UAVs' completion times from (7, 2 s) to (6, 4 s) reduces the maximum time but increases the total time from 9 to 10 s. The optimization of total completion time in multi-U-IRS systems is rarely addressed.

iii) **Tradeoff between EE and total time:** EE and total task completion time are interdependent metrics crucial for system performance and cost. However, the tradeoff between these two key performance indicators remains significantly under-explored in the context of multi-U-IRS-assisted IoT.

1.2 Motivation and Contributions

The aforementioned gaps motivate our work. Specifically, we investigate the fundamental tradeoff between EE and the total task completion time in a multi-U-IRS-assisted IoT data collection system. The main contributions of this paper are fourfold:

- We establish a data collection model for multi-U-IRS-assisted IoT. The expressions for the achievable rate, energy consumption, and system EE are formulated. On this basis, the total task completion time is mathematically characterized. Then, the impacts of UAV-SN association, NoRE, and UAVs trajectories on EE and total mission completion time are analyzed.
- We propose a novel balanced objective function formulated as a weighted sum of the total task completion time and the reciprocal of EE. This formulation allows us to concurrently maximize EE and minimize the total time under practical constraints.
- To solve the resulting non-convex and complex optimization problem, we develop an efficient alternating optimization algorithm. The algorithm decomposes the problem into three subproblems: (i) the UAV-SN association, reformulated as a multi-traveling salesman problem (mTSP) and solved via a genetic algorithm; (ii) the NoRE allocation, solved optimally using a conditional judgment-binary search (CJ-BS) algorithm by leveraging the proved unimodality of the objective function; and (iii) the UAVs trajectories, non-convex constraints are relaxed via slack variables and SCA is utilized to iteratively solve the convexified subproblems.
- Simulation results illustrate the tradeoff between EE and total mission completion time, validating the effectiveness of the proposed scheme. The results demonstrate that the proposed scheme outperforms the static collection benchmark (the UAV hovers above SNs) [8] in terms of mission completion time, highlighting its practical value given the limited endurance and cost of UAVs.

1.3 Structure and Notations

The remainder of this paper is organized as follows: Section 2 presents the system model and problem formulation for multi-U-IRS-assisted data collection in IoT. Section 3 details the iterative algorithm for the joint optimization of UAV-SN association, the optimal NoRE, and UAVs trajectories. Section 4 presents the

numerical results to verify the efficient performance of the proposed algorithm. Finally, Section 5 concludes this paper.

Notations: Scalars are denoted by italic letters, vectors by bold lowercase letters, and matrices by bold uppercase letters. $(\cdot)^H$ and $E(\cdot)$ denote the conjugate transpose of a matrix or vector and the expectation operator, respectively. $\|\cdot\|$ denotes the Euclidean norm, and $diag(\cdot)$ represents a diagonal matrix. $\arg(x)$ denotes a vector with each element being the phase of the corresponding element in x. $\mathbb{R}^{M\times 1}$ represents the space of M-dimensional real-valued vector. $|G|$ denotes the cardinality of set G.

2 Sytem Model and Problem Formulation

2.1 System Model

In this paper, the system model for multi-U-IRS-assisted IoT data collection is illustrated in Fig. 1. The FC is located at coordinates $D = \{0, 0, 0\}$, which is far from the sensors and obstructed by barriers, resulting in no direct line-of-sight (LoS) path between them. We deploy M $(M > 1)$ rotary-wing UAVs, each UAV equipped with IRS to assist relay sensor signals to the FC, where the set of UAVs is denoted as $\{u_m, 1 \le m \le M\}$. Each UAV flies at a constant altitude H, complying with safety regulations and avoiding obstacles. Each U-IRS comprises N reflecting elements, and the NoRE allocated to the SN k is denoted as N_k. A total of k sensors $(K > M)$ are deployed on the ground, with the set of sensors denoted as $\{s_k, 1 \le k \le K\}$. These sensors are stationary with known locations, and their horizontal coordinates are defined as $\mathbf{S}_k \in \mathbb{R}^{2\times 1}$. Each sensor is exclusively served by one U-IRS. Due to the number of sensors exceeding the number of UAVs $(K > M)$, the SNs are partitioned into M disjoint groups. Let $\{G_m, 1 \le m \le M\}$ represent the SN group associated with the UAV U_m, and $|G_m|$ denote the cardinality of the group, $G_m \subseteq \{s_k, 1 \le k \le K\}$. We allocate non-overlapping frequency channels $|G_m|$ to each UAV U_m for collecting data from sensors in G_m. Sensors associated with the same UAV upload data using time-division multiple access (TDMA), eliminating intra-UAV interference. It is reasonable to assume that all SNs aim to upload their task input data as soon as possible. Therefore, the transmission power of each sensor is set to a constant value [32].

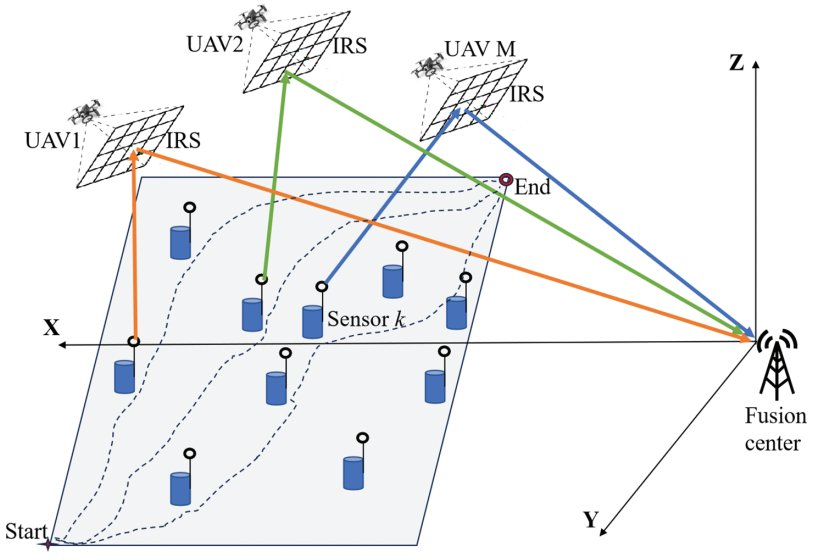

Figure 1: The multi-U-IRS-assisted IoT data collection model

This paper adopts the fly-hover-communicate protocol (FHCP) [33]: where UAVs utilize onboard IRS to assist in SN data collection only during hovering phases, while non-active SNs can enter a sleep mode [34],

thereby extending the lifetime of IoT. Each U-IRS serves one sensor group, and each SN corresponds to a unique hovering point. After completing data collection at one hovering point, the UAV proceeds to the next one, e.g., the UAV U_m exclusively collects data from SNs in G_m, with $|G_m|$ hover points involved in this process. Consequently, the trajectory of the UAV U_m starts from the start point, traverses all the hovering point $|G_m|$, finally flies to the end point. The 2D coordinates of the UAVs' start and end points are predefined as $\mathbf{q}_I, \mathbf{q}_F \in \mathbb{R}^{2\times 1}$, respectively. Therefore, determining the UAVs' trajectories requires solving for the optimal hovering point positions.

We define $\lambda_{m,k} \in \{0,1\}$ as the SN-UAV association variable [35]. If the SN s_k is associated to the UAV U_m, $\lambda_{m,k} = 1$; otherwise, $\lambda_{m,k} = 0$. So $G_m = \{s_k \,|\lambda_{m,k} = 1, \forall k, 1 \le m \le M\}$, ensure exclusive association. Since a SN is only served by one U-IRS, we can get $\sum_{m=1}^{M} \lambda_{m,k} = 1$. $\pi_m = (\pi_{m,1}, \pi_{m,2}, \cdots, \pi_{m,|G_m|})$ represents the visiting order of the SNs, the visit sequence of SNs in G_m can be expressed as $(s_{\pi_{m,1}}, s_{\pi_{m,2}}, \cdots, s_{\pi_{m,|G_m|}})$. Define $\mathbf{q}_{\pi_{m,l}} \in \mathbb{R}^{2\times 1}, 1 \le l \le |G_m|$ as the 2-D coordinate of the hover point corresponding to the SN $s_{\pi_{m,l}}$ associated with the UAV U_m. The start and end point of the UAV U_m are defined as $\mathbf{q}_{\pi_{m,0}} = \mathbf{q}_I$ and $\mathbf{q}_{\pi_{m,|G_m|+1}} = \mathbf{q}_F$.

For the SN $s_{\pi_{m,l}}$, the received signal at the FC is

$$y_{\pi_{m,l}} = \mathbf{g}^H_{N_{m,l},FC} \Theta \mathbf{g}_{l,N_{m,l}} \sqrt{P_s} x + \omega_{\pi_{m,l}} \tag{1}$$

where P_s is the transmit power of the SN $s_{\pi_{m,l}}$. Without loss of generality, hypothetically $E(x) = 0$, $E(x^2) = 1$. $\omega_{\pi_{m,l}} \sim CN(0, \sigma^2)$ is the Gaussian noise with zero mean and variance σ^2. $N_{m,l}$ is the NoRE used by the SN $s_{\pi_{m,l}}$, $1 \le N_{m,l} \le N$. Let $\hat{N}_{m,l}$ denotes the index of a specific reflecting element in use, with $\hat{N}_{m,l} \in \{1, 2, \cdots, N_{m,l}\}$. $\mathbf{g}^H_{N_{m,l},FC} = \left[g_{1,FC}, g_{2,FC}, \cdots, g_{N_{m,l},FC}\right]$ represents the channel power gain from the reflecting element to the FC, $\mathbf{g}^H_{N_{m,l},FC} \in \mathbb{C}^{1\times N}$. $\mathbf{g}_{l,N_{m,l}} = \left[g_{l,1}, g_{l,2}, \cdots, g_{l,N_{m,l}}\right]^H$ represents the channel power gain from the SN $s_{\pi_{m,l}}$ to the reflecting element, $\mathbf{g}_{l,N_{m,l}} \in \mathbb{C}^{N\times 1}$. The channel power gain can be expressed as [36]: $g_{\hat{N}_{m,l},FC} = \sqrt{\rho_0 d^{-\alpha}_{\hat{N}_{m,l},FC}}\varsigma_l$, $g_{l,\hat{N}_{m,l}} = \sqrt{\rho_0 d^{-\alpha}_{l,\hat{N}_{m,l}}}\varsigma_l$, where ρ_0 is the average channel power gain at a reference distance of 1 meter, $d_{l,\hat{N}_{m,l}}$ represents the distance between SN $s_{\pi_{m,l}}$ and the reflecting element $\hat{N}_{m,l}$ in the IRS, $d_{l,\hat{N}_{m,l}} = \sqrt{H^2 + \left\|\mathbf{q}_{\pi_{m,l}} - \mathbf{S}_{\pi_{m,l}}\right\|^2}$. $d_{N_{m,l},FC} = \sqrt{H^2 + \left\|\mathbf{q}_{\pi_{m,l}}\right\|^2}$. $d_{\hat{N}_{m,l},FC}$ represents the distance from the reflecting element $\hat{N}_{m,l}$ in the IRS to the FC (approximated as UAV-to-FC distance due to small IRS size), $d_{\hat{N}_{m,l},FC} = \sqrt{H^2 + \left\|\mathbf{q}_{\pi_{m,l}}\right\|^2}$. α represents the path loss exponent. ς_k describes the medium and small-scale Rayleigh fading component of the channel, which is an exponential variable that satisfies the independent and same distribution, with $E\left(|\varsigma_k|^2\right) = 1$. Define $\theta_{\hat{N}_{m,l}} = e^{j\theta_{\hat{N}_{m,l}}}$, $\Theta = diag\left[\theta_1, \theta_2, \cdots, \theta_{\hat{N}_{m,l}}, \cdots, \theta_{N_{m,l}}\right]$. $\theta_{\hat{N}_{m,l}} \in [0, 2\pi)$ is the phase shift of the reflecting element $\hat{N}_{m,l}$, which can be expressed as [37]: $\theta_{\hat{N}_{m,l}} = -\arg(g_{\hat{N}_{m,l},FC} g_{l,\hat{N}_{m,l}})$.

The instantaneous achievable rate corresponding to the SN $s_{\pi_{m,l}}$ can be expressed as a function of the NoRE $N_{m,l}$ and the position of the hover point $\mathbf{q}_{\pi_{m,l}}$.

$$R_{\pi_{m,l}}\left\{N_{m,l}, \mathbf{q}_{\pi_{m,l}}\right\} = B\log_2\left(1 + \frac{P_s\left(\sum_{\hat{N}_{m,l}=1}^{N_{m,l}} \left|g_{\hat{N}_{m,l},FC} g_{l,\hat{N}_{m,l}}\right|\right)^2}{\sigma^2}\right) \tag{2}$$

where B is the bandwidth allocated to the UAV U_m. The frequency-division multiplexing access mechanism is adopted to avoid inter-UAV interference, which assumes that different UAVs operate on distinct frequencies during data collection and transmission.

The SE is defined as

$$SE_{\pi_{m,l}}\left\{N_{m,l},\mathbf{q}_{\pi_{m,l}}\right\}=\frac{R_{\pi_{m,l}}\left\{N_{m,l},\mathbf{q}_{\pi_{m,l}}\right\}}{B}=\log_2\left(1+\frac{P_s\left(\sum_{\hat{N}_{m,l}=1}^{N_{m,l}}\left|g_{\hat{N}_{m,l},FC}g_{l,\hat{N}_{m,l}}\right|\right)^2}{\sigma^2}\right) \tag{3}$$

2.2 EE Model

The total energy consumption of the system during UAVs-assisted service comprises the following components: the energy consumption for traveling of the UAVs, the total UAVs hovering energy consumption, the energy consumption of reflecting element in IRS for phase shifting, the energy consumption of SNs (including signal transmission and intrinsic circuit power), the intrinsic energy consumption of FC. The total energy consumption can be formulated as

$$\begin{aligned}E_m&=E_{UAV,f}+E_{UAV,h}+E_{IRS}+E_{G_m}+E_{FC}\\&=E_p^{mr}\sum_{l=1}^{|G_m|+1}\left\|\mathbf{q}_{\pi_{m,l}}-\mathbf{q}_{\pi_{m,l-1}}\right\|+\sum_{l=1}^{|G_m|}\tau_{\pi_{m,l}}\left(P_{UAV}(0)+N_{m,l}P_{IRS}+\eta P_s+P_{C,\pi_{m,l}}+P_{FC}\right)\\&=E_p^{mr}\sum_{l=1}^{|G_m|+1}\left\|\mathbf{q}_{\pi_{m,l}}-\mathbf{q}_{\pi_{m,l-1}}\right\|+\sum_{l=1}^{|G_m|}\tau_{\pi_{m,l}}\left(N_{m,l}P_{IRS}+P_{else,\pi_{m,l}}\right)\end{aligned} \tag{4}$$

The calculation methods for E_p^{mr} and $P_{UAV}(V)$ refer to [33]. E_p^{mr} is the maximum-range (MR) propulsion energy consumption of the UAV per unit traveling distance in Joule/meter, representing the minimum UAV energy consumption per unit traveling distance. $P_{UAV}(V)$ is the power consumption of the rotor-wing UAV, when $V=0$, and $P_{UAV}(0)$ denotes the UAV's hovering power consumption when the UAV hovers. $P_{else,\pi_{m,l}}=P_{UAV}(0)+\eta P_s+P_{C,\pi_{m,l}}+P_{FC}$, $\tau_{\pi_{m,l}}$ is the hovering time of the UAV U_m corresponding to the SN $s_{\pi_{m,l}}$. P_{IRS} is the power consumption when the reflecting elements of IRS provide the phase shift. η denotes the power amplifier efficiency, $P_{C,\pi_{m,l}}$ is the intrinsic circuit power consumption of the SN $s_{\pi_{m,l}}$, and P_{FC} represents the intrinsic power consumption of the FC.

The total energy consumption and EE of the system can be expressed as (5) and (6), respectively, where $Q_{\pi_{m,l}}$ is data amount that need to be collected from the SN $s_{\pi_{m,l}}$.

$$E_{total}=\sum_{m=1}^{M}E_m=E_p^{mr}\sum_{m=1}^{M}\sum_{l=1}^{|G_m|+1}\left\|\mathbf{q}_{\pi_{m,l}}-\mathbf{q}_{\pi_{m,l-1}}\right\|+\sum_{m=1}^{M}\sum_{l=1}^{|G_m|}\tau_{\pi_{m,l}}\left(N_{m,l}P_{IRS}+P_{else,\pi_{m,l}}\right) \tag{5}$$

$$EE_{total}=\frac{\sum_{m=1}^{M}\sum_{l=1}^{|G_m|}Q_{\pi_{m,l}}}{E_p^{mr}\sum_{m=1}^{M}\sum_{l=1}^{|G_m|+1}\left\|\mathbf{q}_{\pi_{m,l}}-\mathbf{q}_{\pi_{m,l-1}}\right\|+\sum_{m=1}^{M}\sum_{l=1}^{|G_m|}\tau_{\pi_{m,l}}\left(N_{m,l}P_{IRS}+P_{else,\pi_{m,l}}\right)} \tag{6}$$

2.3 Mission Completion Time

In multi-U-IRS-assisted IoT data collection, the total mission completion time comprises two components: (1) The flight time of UAVs: The time required for UAVs to fly from the starting point, traverse all hovering points in sequence, and finally reach the endpoint. (2) The hovering time of UAVs: The time spent at each hovering point, during which the IRS in UAVs assists in transmitting SN signals to the FC. After completing data transmission from the associated SNs, UAVs terminates hovering and proceeds to the next hovering point immediately. Set T_f to the UAVs total flight time, it is associated with the total flight distance of the UAVs. So the total mission completion time can be expressed as

$$T_f = \frac{\sum_{m=1}^{M} \sum_{l=1}^{|G_m|+1} \left\| \mathbf{q}_{\pi_{m,l}} - \mathbf{q}_{\pi_{m,l-1}} \right\|}{V_{mr}} \tag{7}$$

where V_{mr} is the MR speed, which is the minimum UAV flight speed with minimal energy consumption under the FHCP [33].

Let T_h be the total hovering time of the UAVs, which is related to the UAVs hovering time at each hovering point and can be expressed as

$$T_h = \sum_{m=1}^{M} \sum_{l=1}^{|G_m|} \tau_{\pi_{m,l}} \tag{8}$$

Thus, the total task completion time can be expressed as [35]

$$T_{total} = T_f + T_h = \frac{\sum_{m=1}^{M} \sum_{l=1}^{|G_m|+1} \left\| \mathbf{q}_{\pi_{m,l}} - \mathbf{q}_{\pi_{m,l-1}} \right\|}{V_{mr}} + \sum_{m=1}^{M} \sum_{l=1}^{|G_m|} \tau_{\pi_{m,l}} \tag{9}$$

As shown in (9), both T_{total} and EE are associated with the flight distance and hovering time of UAVs, indicating that these two objectives are highly coupled.

2.4 Problem Formulation

Unlike single-U-IRS-assisted IoT data collection, in multi-U-IRS-assisted IoT data collection, we must consider both maximizing EE and minimizing the total mission completion time to fully demonstrate the advantages of multi-UAV systems. Eqs. (6) and (9) reveal that EE and mission completion time are closely related to three optimization parameters: the SN-UAV association $\{\lambda_{m,k}\}$, NoRE $\{N_{m,l}\}$, and the hovering point positions $\left\{\mathbf{q}_{\pi_{m,l}}\right\}$. In this paper, we aim to achieve a balanced optimization of EE and total mission completion time by jointly optimizing these three parameters. To facilitate analysis, we define as (10).

$$\chi = \frac{1}{EE_{total}} = \frac{E_p^{mr} \sum_{m=1}^{M} \sum_{l=1}^{|G_m|+1} \left\| \mathbf{q}_{\pi_{m,l}} - \mathbf{q}_{\pi_{m,l-1}} \right\| + \sum_{m=1}^{M} \sum_{l=1}^{|G_m|} \tau_{\pi_{m,l}} (N_{m,l} P_{IRS} + P_{else,\pi_{m,l}})}{\sum_{m=1}^{M} \sum_{l=1}^{|G_m|} Q_{\pi_{m,l}}} \tag{10}$$

Thus the problem of EE maximization is transformed into the minimization problem of χ.

According to the above analysis, the problem can be formulated as a multi-objective optimization problem (P1).

$$(\text{p1}): \min_{\{\lambda_{m,k}\},\{N_k\},\left\{\mathbf{q}_{\pi_{m,l}}\right\}} \chi \tag{11a}$$

$$\min_{\{\lambda_{m,k}\},\{N_k\},\left\{\mathbf{q}_{\pi_{m,l}}\right\}} T_{total} \tag{11b}$$

$$\text{s.t.} \sum_{m=1}^{M} \lambda_{m,k} = 1,\ 1 \le k \le K,\ \forall k \tag{11c}$$

$$G_m = \{s_k \,|\lambda_{m,k} = 1,\ \forall k,\ 1 \le m \le M\} \tag{11d}$$

$$\lambda_{m,k} \in \{0,\ 1\},\ \forall m,\ k \tag{11e}$$

$$1 \le N_{m,l} \le N,\ \forall m,\ l \tag{11f}$$

$$\mathbf{q}_{\pi_{m,0}} = \mathbf{q}_I,\ \mathbf{q}_{\pi_{m,|G_m|+1}} = \mathbf{q}_F \tag{11g}$$

$$\tau_{\pi_{m,l}}\left(\eta P_s + P_{C,\pi_{m,l}}\right) \le E_{\pi_{m,l},\max},\ \forall m, l \tag{11h}$$

$$E_p^{mr} \sum_{l=1}^{|G_m|+1} \left\|\mathbf{q}_{\pi_{m,l}} - \mathbf{q}_{\pi_{m,l-1}}\right\| + \sum_{l=1}^{|G_m|} \tau_{\pi_{m,l}}\left(P_{UAV}(0) + N_{m,l}P_{IRS}\right) \le E_{m,\max},\ \forall m, l \tag{11i}$$

$$\tau_{\pi_{m,l}} B \log_2\left(1 + \frac{P_s\left(\sum_{\hat{N}_{m,l}=1}^{N_{m,l}} \left|g_{\hat{N}_{m,l},FC} g_{l,\hat{N}_{m,l}}\right|\right)^2}{\sigma^2}\right) \ge Q_{\pi_{m,l}},\ \forall m, l \tag{11j}$$

Eq. (11c)–(11e) indicates the association between the UAV and SN. Eq. (11f) represents the constraint on the NoRE. It is the upper bound of the NoRE, which means that the number of allocated elements can not exceed the most NoRE that the UAV carried. Eq. (11g) defines the UAV trajectory's start and end point constraints. Eq. (11h) indicates the energy budget constraint of the SN, where $E_{\pi_{m,l},\max}$ denotes the maximum energy budget of a SN $s_{\pi_{m,l}}$. Eq. (11i) represents the UAV energy constraint. Due to the limited endurance time of UAVs, the mission must be completed within the UAV's operational duration. Eq. (11j) represents the throughput constraint, ensuring complete data collection from all SNs.

Lemma 1: At the optimal solution to problem (P1), we have

$$\tau_{\pi_{m,l}} B \log_2\left(1 + \frac{P_s\left(\sum_{\hat{N}_{m,l}=1}^{N_{m,l}} \left|g_{\hat{N}_{m,l},FC} g_{l,\hat{N}_{m,l}}\right|\right)^2}{\sigma^2}\right) = Q_{\pi_{m,l}},\ \forall m, l \tag{12}$$

Proof: Lemma 1 can be shown by contradiction. If there is an optimal solution $\tau^*_{\pi_{m,l}}$ making $\tau^*_{\pi_{m,l}} B\log_2(1+\frac{P_s\left(\sum_{\dot{N}_{m,l}=1}^{N_{m,l}}\left|g_{\dot{N}_{m,l},FC}g_{l,\dot{N}_{m,l}}\right|\right)^2}{\sigma^2}) > Q_{\pi_{m,l}}, \forall m,l$. We can find $\tau'_{\pi_{m,l}} < \tau^*_{\pi_{m,l}}$ to satisfy these constraints. In other words, $\tau^*_{\pi_{m,l}}$ can be decreased with other variables fixed, then χ and T_{total} decrease, and all other constraints are still satisfied, contradicting Pareto optimality, the lemma is proved.□

As revealed by Lemma 1, for (P1), the optimal hovering time in (P1) exactly matches the time required to complete data transmission from the SNs. Upon completing data collection, the UAV ceases hovering and proceeds to the next hovering point along a straight trajectory. We assume that all SNs have identical data upload requirements and the number of information bits that need to be collected from every SN is $\tilde{Q}$, so we derive $\sum_{m=1}^{M}\sum_{l=1}^{|G_m|} Q_{\pi_{m,l}} = K\cdot\tilde{Q}$. Following lemma 1, the hovering time of the UAV U_m at the hover point associated with the SN $s_{\pi_{m,l}}$ can be expressed as

$$\tau_{\pi_{m,l}}\left\{N_{m,l},\mathbf{q}_{\pi_{m,l}}\right\} = \frac{\tilde{Q}}{R_{\pi_{m,l}}\left\{N_{m,l},\mathbf{q}_{\pi_{m,l}}\right\}} \tag{13}$$

As shown in the expression for EE in (6), the EE depends on the UAV-SN association $\{\lambda_{m,k}\}$, NoRE $\{N_{m,l}\}$, and hovering point position $\left\{\mathbf{q}_{\pi_{m,l}}\right\}$. Similarly, the total mission completion time is also influenced by these three parameters. Taking the NoRE as an example: (2) indicates that the achievable rate of the associated SN increases with NoRE, thereby reducing the UAV hovering time required for transmit the target data amount $\tilde{Q}$ and shortening the total mission completion time. However, increasing the NoRE also raises energy consumption, which negatively impacts the system EE. This implies the NoRE minimizing mission completion time does not necessarily correspond to the maximum EE. Similar tradeoff analyses apply to the other two parameters. Therefore, a fundamental tradeoff between EE and mission completion time can be explored. To characterize the tradeoff, we define a weighted sum as

$$\Lambda_\omega = \omega_{wf}\psi_{cf}\chi + (1-\omega_{wf})T_{total} \tag{14}$$

where $0 \le \omega_{wf} \le 1$ is the weighting factor, ψ_{cf} is the compensation factor for χ. Since the χ and T_{total} are at different levels, ψ_{cf} is therefore introduced to scale these two terms to a comparable numerical range, this enables the two variables to be of the same order of magnitude, ensuring that the weight $0 \le \omega_{wf} \le 1$ can effectively and intuitively adjust the tradeoff between energy efficiency and total mission completion time. Finally, (P1) is reformulated as

$$\text{(P2):} \min_{\{\lambda_{m,k}\},\{N_k\},\left\{\mathbf{q}_{\pi_{m,l}}\right\}} \Lambda_\omega \tag{15a}$$

$$\text{s.t. (11c)–(11i)} \tag{15b}$$

$$0 \le \omega_{wf} \le 1 \tag{15c}$$

According to (P2) and (12), ω_{wf} and $(1-\omega_{wf})$ determine the priority of enlarging the system's EE and decreasing the total mission completion time, respectively. Note that the case of $\omega_{wf}=1$ is equivalent to the χ minimization problem, which equates to the EE maximization problem. $\omega_{wf}=0$ is equivalent to the total mission completion time minimization problem. Obviously, we can always obtain the unique optimal tradeoff between the EE and the total mission completion time for any ω_{wf}.

3 Algorithm Design

(P2) is a constrained combinatorial optimization problem, where the objective function Λ_ω depends on UAV-SN association $\{\lambda_{m,k}\}$, NoRE $\{N_{m,l}\}$, and hovering point positions $\left\{\mathbf{q}_{\pi_{m,l}}\right\}$. The coupling of these three variables in constraints (11g)–(11i), along with the non-convexity of (11i) and $\lambda_{m,k}$ is a binary function in (11d), renders (P2) intractable for direct optimization. We decompose (P2) into three sub-problems to optimize the UAV-SN association optimization, NoRE, and the hovering point position separately. For each sub-problem, we assume the other variables are fixed and optimize only the targeted variable. The alternating optimization of these three variables is then employed to solve (P2).

To facilitate subsequent analysis, we expand and reorganize the mathematical expression of Λ_ω, and combine like terms. The reformulated expression of Λ_ω is given as

$$
\begin{aligned}
\Lambda_\omega &= \omega_{wf}\psi_{cf}\chi + (1-\omega_{wf})T_{total} \\
&= \omega_{wf}\psi_{cf}\frac{E_p^{mr}\sum_{m=1}^{M}\sum_{l=1}^{|G_m|+1}\left\|\mathbf{q}_{\pi_{m,l}}-\mathbf{q}_{\pi_{m,l-1}}\right\| + \sum_{k=1}^{K}\tau_k(N_k P_{IRS}+P_{else,k})}{K\cdot\tilde{Q}} \\
&\quad +(1-\omega_{wf})\left(\sum_{m=1}^{M}\sum_{l=1}^{|G_m|+1}\frac{\left\|\mathbf{q}_{\pi_{m,l}}-\mathbf{q}_{\pi_{m,l-1}}\right\|}{V_{mr}} + \sum_{m=1}^{M}\sum_{l=1}^{|G_m|}\tau_{\pi_{m,l}}\right) \\
&= \left(\frac{\omega_{wf}\psi_{cf}E_p^{mr}}{K\cdot\tilde{Q}} + \frac{1-\omega_{wf}}{V_{mr}}\right)\sum_{m=1}^{M}\sum_{l=1}^{|G_m|+1}\left\|\mathbf{q}_{\pi_{m,l}}-\mathbf{q}_{\pi_{m,l-1}}\right\| \\
&\quad + \sum_{m=1}^{M}\sum_{l=1}^{|G_m|}\tau_{\pi_{m,l}}\left(\frac{\omega_{wf}\psi_{cf}(N_{m,l}P_{IRS}+P_{else,\pi_{m,l}})}{K\cdot\tilde{Q}} + (1-\omega_{wf})\right) \\
&= \underbrace{\left(\frac{\omega_{wf}\psi_{cf}E_p^{mr}}{K\cdot\tilde{Q}} + \frac{1-\omega_{wf}}{V_{mr}}\right)\sum_{m=1}^{M}\sum_{l=1}^{|G_m|+1}\left\|\mathbf{q}_{\pi_{m,l}}-\mathbf{q}_{\pi_{m,l-1}}\right\|}_{part\ 1} \\
&\quad + \underbrace{\sum_{m=1}^{M}\sum_{l=1}^{|G_m|}\frac{\tilde{Q}}{B\log_2\left(1+\frac{P_s\left(\sum_{N_{m,l}=1}^{N}\left|g_{N_{m,l},FC}g_{l,N_{m,l}}\right|\right)^2}{\sigma^2}\right)}\left(\frac{\omega_{wf}\psi_{cf}(N_{m,l}P_{IRS}+P_{else,\pi_{m,l}})}{K\cdot\tilde{Q}} + (1-\omega_{wf})\right)}_{part\ 2}
\end{aligned}
\tag{16}
$$

Eq. (16) intuitively illustrates the correlation among UAV-SN association $\{\lambda_{m,k}\}$, NoRE $\{N_{m,l}\}$, hovering point position $\left\{\mathbf{q}_{\pi_{m,l}}\right\}$, and the objective function Λ_ω, thereby facilitating subsequent analysis.

The alternating optimization process proceeds as follows.

3.1 Algorithm Design

When the NoRE $\{N_{m,l}\}$ and the hovering point $\left\{\mathbf{q}_{\pi_{m,l}}\right\}$ are given, the achievable rate of the associated SN and the corresponding UAV hovering time become fixed. Consequently, part 2 in (16) becomes a constant. For the UAV-SN association $\{\lambda_{m,k}\}$ requiring optimization, we only need to analyze part 1 in (16). Under

these conditions, (P2) can be reformulated as

$$\text{(P3)}: \min_{\{\lambda_{m,k}\}} \left(\frac{\omega_{wf}\psi_{cf}E_p^{mr}}{K\cdot\tilde{Q}} + \frac{1-\omega_{wf}}{V_{mr}}\right) \sum_{m=1}^{M} \sum_{l=1}^{|G_m|+1} \left\| \mathbf{q}_{\pi_{m,l}} - \mathbf{q}_{\pi_{m,l-1}} \right\| \tag{17a}$$

$$\text{s.t.} \quad (11c)\text{–}(11e), (11g), (15c) \tag{17b}$$

The objective function of (P3) can be expanded as

$$\begin{aligned} &\left(\frac{\omega_{wf}\psi_{cf}E_p^{mr}}{K\cdot\tilde{Q}} + \frac{1-\omega_{wf}}{V_{mr}}\right) \sum_{m=1}^{M} \sum_{l=1}^{|G_m|+1} \left\| \mathbf{q}_{\pi_{m,l}} - \mathbf{q}_{\pi_{m,l-1}} \right\| \\ &= \left(\frac{\omega_{wf}\psi_{cf}E_p^{mr}}{K\cdot\tilde{Q}} + \frac{1-\omega_{wf}}{V_{mr}}\right) \left(\sum_{l=1}^{|G_1|+1} \left\| \mathbf{q}_{\pi_{1,l}} - \mathbf{q}_{\pi_{1,l-1}} \right\| + \sum_{l=1}^{|G_2|+1} \left\| \mathbf{q}_{\pi_{2,l}} - \mathbf{q}_{\pi_{2,l-1}} \right\| + \cdots + \sum_{l=1}^{|G_M|+1} \left\| \mathbf{q}_{\pi_{M,l}} - \mathbf{q}_{\pi_{M,l-1}} \right\| \right) \end{aligned} \tag{18}$$

As shown in (18), the minimization of the objective function in optimization problem (P3) corresponds to minimizing the flight distances of UAVs serving different SN groups, which constitutes a multiple Traveling Salesman Problem (m-TSP) with predetermined initial and final locations. Specifically, this involves multi-salesmen starting from predefined origins, each visiting a distinct subset of cities (where each city is visited exactly once by one salesman), and all salesmen ultimately arriving at predetermined destinations. The goal is to find the solution that minimizes the total travel distance. Since the m-TSP is NP-hard, optimization problem (P3) also falls into the NP-hard category. Consequently, genetic algorithm can obtain an efficient approximate solution for (P3).

3.2 Optimizing NoRE

When given the UAV-SN association $\{\lambda_{m,k}\}$ and hover point position $\left\{\mathbf{q}_{\pi_{m,l}}\right\}$, the UAV trajectory and the SN groups associated with each UAV are determined, and the visit sequence of SNs within each assigned group becomes deterministic. Therefore, part 1 in (16) becomes deterministic. For the NoRE $\{N_{m,l}\}$ requiring optimization, we only need to focus on minimizing part 2 in (16). Under this condition, (P2) can be reformulated as (P4).

$$\text{(P4)}: \min_{\{N_{m,l}\}} \quad \sum_{m=1}^{M} \sum_{l=1}^{|G_m|} \frac{\tilde{Q}}{B\log_2\left(1+\frac{P_s\left(\sum_{n=1}^{N_{m,l}} |g_{n,FC}g_{l,n}|\right)^2}{\sigma^2}\right)} \times \left(\frac{\omega_{wf}\psi_{cf}(N_{m,l}P_{IRS}+P_{else,\pi_{m,l}})}{K\cdot\tilde{Q}} + (1-\omega_{wf})\right) \tag{19a}$$

$$\text{s.t.} \quad (11f), (11h)\text{–}(11i), (15c) \tag{19b}$$

By expanding the objective function in (P4), we can get (20), which is shown at the bottom of page 9. Where $\gamma_{m,l} = \frac{\omega_{wf}\psi_{cf}P_{IRS}}{K\cdot\tilde{Q}}$, $\beta_{N_{m,l}} \geq \beta_{N_{m,l}+1}$, $\delta = \frac{P_s}{\sigma^2}$, $\beta_{N_{m,l}} = \left|g_{N_{m,l},FC}g_{l,N_{m,l}}\right|$, and in descending order, that is

$\beta_{N_{m,l}} \geq \beta_{N_{m,l}+1}$.

$$\sum_{m=1}^{M}\sum_{l=1}^{|G_m|}\frac{\tilde{Q}}{B\log_2\left(1+\frac{P_s\left(\sum_{N_{m,l}=1}^{N}\left|g_{N_{m,l},FC}g_{l,N_{m,l}}\right|\right)^2}{\sigma^2}\right)}\left(\frac{\omega_{wf}\psi_{cf}\left(N_{m,l}P_{IRS}+P_{else,\pi_{m,l}}\right)}{K\cdot\tilde{Q}}+\left(1-\omega_{wf}\right)\right)$$

$$=\sum_{m=1}^{M}\sum_{l=1}^{|G_m|}\frac{\tilde{Q}}{B\log_2\left(1+\frac{P_s\left(\sum_{N_{m,l}=1}^{N}\left|g_{N_{m,l},FC}g_{l,N_{m,l}}\right|\right)^2}{\sigma^2}\right)}\left(N_{m,l}\frac{\omega_{wf}\psi_{cf}P_{IRS}}{K\cdot\tilde{Q}}+\left(\frac{\omega_{wf}\psi_{cf}P_{else,\pi_{m,l}}}{K\cdot\tilde{Q}}+\left(1-\omega_{wf}\right)\right)\right)$$

$$=\sum_{m=1}^{M}\sum_{l=1}^{|G_m|}\frac{\tilde{Q}}{B\log_2\left(1+\delta\left(\sum_{N_{m,l}=1}^{N}\beta_{N_{m,l}}\right)^2\right)}\left(N_{m,l}\gamma_{m,l}+\zeta_{m,l}\right)$$

$$=\underbrace{\frac{\tilde{Q}}{B\log_2\left(1+\delta\left(\sum_{N_{1,1}=1}^{N}\beta_{N_{1,1}}\right)^2\right)}\left(N_{1,1}\gamma_{1,1}+\zeta_{1,1}\right)}_{\text{part (1,1)}}+\underbrace{\frac{\tilde{Q}}{B\log_2\left(1+\delta\left(\sum_{N_{1,2}=1}^{N}\beta_{N_{1,2}}\right)^2\right)}\left(N_{1,2}\gamma_{1,2}+\zeta_{1,2}\right)}_{\text{part (1,2)}}+\cdots+$$

$$\underbrace{\frac{\tilde{Q}}{B\log_2\left(1+\delta\left(\sum_{N_{M,|G_m|}=1}^{N}\beta_{N_{M,|G_m|}}\right)^2\right)}\left(N_{M,|G_m|}\gamma_{M,|G_m|}+\zeta_{M,|G_m|}\right)}_{\text{part (M,}|G_m|\text{)}} \tag{20}$$

First, we select part (m, l) in (20) for analysis, subsequently extending the methodology to the aggregate sum of all parts. According to our prior work [38], when $\delta\left(\sum_{N_{m,l}=1}^{N}\beta_{N_{m,l}}\right)^2 \geq 1$, $R_{\pi_{m,l}}(N_{m,l}+1)-R_{\pi_{m,l}}(N_{m,l}) \geq R_{\pi_{m,l}}(N_{m,l}+2)-R_{\pi_{m,l}}(N_{m,l}+1)$. Proposition 1: $F(N_{m,l})=\frac{\tilde{Q}}{B\log_2\left(1+\delta\left(\sum_{N_{m,l}=1}^{N}\beta_{N_{m,l}}\right)^2\right)}\left(N_{m,l}\gamma_{m,l}+\zeta_{m,l}\right)$ is a unimodal function.

Proof: See Appendix A.□

According to proposition 1, it can be seen that $F(N_{m,l})$ is a unimodal function, and the CS-BJ algorithm in our existing research [38] is applied to solve the optimal NoRE $\tilde{N}_{m,l}$ to obtain the minimum value of $F(N_{m,l})$. Similarly, in (18), we can use the CS-BJ algorithm to solve the minimum value of each part, thus obtaining the minimum value of the objective function in (P4). The CS-BJ algorithm for (P4) is summarized in Algorithm 1.

Algorithm 1: CS-BJ algorithm for solving (P4)

1: Initialize UAV-SN association $\{\lambda_{m,k}\}$ and the hovering position $\left\{\mathbf{q}_{\pi_{m,l}}\right\}$. Calculate the range of the NoRE $\underline{N}$ and $\tilde{N}$ according to the constraints.
2: for $N_{m,l} = \underline{N} : 1 : \overline{N}$;
3: if $F\left(\overline{N}\right) \leq F\left(\overline{N}-1\right)$
4: $F_{\min}\left(\tilde{N}\right) = F\left(\overline{N}\right)$
5: $N^*_{m,l} = \overline{N}$
6: else
7: if $F\left(\underline{N}\right) \leq F\left(\underline{N}+1\right)$
8: $F_{\min}\left(\tilde{N}\right) = F\left(\underline{N}\right)$
9: $N^*_{m,l} = \underline{N}$
10: else
11: $N^*_{m,l}$ is solved by the Binary Search algorithm;
12: $F_{\min}\left(N_{m,l}\right) = F\left(N^*_{m,l}\right)$
13: end
14: end
15: Output: The optimal NoRE $N^*_{m,l}$.

$F(N_{m,l})$ can be written as

$$F(N_{m,l}) = \frac{\tilde{Q}}{B\log_2(1+\delta\left(\sum\limits_{N_{m,l}=1}^{N}\beta_{N_{m,l}}\right)^2)}(N_{m,l}\gamma_{m,l}+\zeta_{m,l}) = \frac{\tilde{Q}\gamma_{m,l}}{B}\cdot\frac{N_{m,l}+\frac{\zeta_{m,l}}{\gamma_{m,l}}}{\log_2(1+\delta\left(\sum\limits_{N_{m,l}=1}^{N}\beta_{N_{m,l}}\right)^2)} \tag{21}$$

From (21), it is evident that as a unimodal function, the peak of the unimodal function $F(N_{m,l})$ corresponds to a specific NoRE $\tilde{N}_{m,l}$ and $\frac{\zeta_{m,l}}{\gamma_{m,l}}$. Different values of ω_{wf} yield distinct $\frac{\zeta_{m,l}}{\gamma_{m,l}}$, and then obtain distinct optimal NoRE $\tilde{N}_{m,l}$, which also affect the value of Λ_ω. Thereby ω_{wf} is critical to achieve the balance between EE and the total mission completion time. The impact of ω_{wf} is analyzed in the simulations.

3.3 Optimizing UAV Trajectory

Given UAV-SN association $\{\lambda_{m,k}\}$ and NoRE $\{N_{m,l}\}$, the SN group associated with each UAV is also determined, and the visit sequence of SNs within each SN group and NoRE used by each SN is determined. According to (16), the hover point $\left\{\mathbf{q}_{\pi_{m,l}}\right\}$ is related to both part 1 and part 2. Compared to (P2), the constraints involved in $\{\lambda_{m,k}\}$ and $\{N_{m,l}\}$ need not be considered. So (P2) can be rewritten as

$$(\text{P5}): \min_{\left\{\mathbf{q}_{\pi_{m,l}}\right\}} \Lambda_\omega \tag{22a}$$

$$\text{s.t. (11g)–(11i), (15c)} \tag{22b}$$

$$
\begin{aligned}
\Lambda_{\omega} &= \left(\frac{\omega_{wf}\psi_{cf}E_p^{mr}}{K\cdot\tilde{Q}} + \frac{1-\omega_{wf}}{V_{mr}}\right)\sum_{m=1}^{M}\sum_{l=1}^{|G_m|+1}\left\|\mathbf{q}_{\pi_{m,l}} - \mathbf{q}_{\pi_{m,l-1}}\right\| \\
&+ \sum_{m=1}^{M}\sum_{l=1}^{|G_m|}\frac{\tilde{Q}}{B\log_2\left(1+\frac{P_s\left(\sum_{N_{m,l}=1}^{N_{m,l}}\left|g_{N_{m,l},FC}g_{l,N_{m,l}}\right|\right)^2}{\sigma^2}\right)}\left(\frac{\omega_{wf}\psi_{cf}\left(N_{m,l}P_{IRS}+P_{else,\pi_{m,l}}\right)}{K\cdot\tilde{Q}} + \left(1-\omega_{wf}\right)\right) \\
&= \ell\sum_{m=1}^{M}\sum_{l=1}^{|G_m|+1}\left\|\mathbf{q}_{\pi_{m,l}} - \mathbf{q}_{\pi_{m,l-1}}\right\| + \sum_{m=1}^{M}\sum_{l=1}^{|G_m|}\frac{\tilde{Q}(N_{m,l}\gamma_{m,l}+\zeta_{m,l})}{B\log_2\left(1+\frac{\delta\left(\sum_{N_{m,l}=1}^{N_{m,l}}h_{N_{m,l},m,l}\right)^2}{\left(d_{l,N_{m,l}}d_{N_{m,l},FC}\right)^{\alpha}}\right)} \\
&= \ell\sum_{l=1}^{|G_1|+1}\left\|\mathbf{q}_{\pi_{1,l}} - \mathbf{q}_{\pi_{1,l-1}}\right\| + \sum_{l=1}^{|G_1|}\frac{\tilde{Q}(N_{1,l}\gamma_{1,l}+\zeta_{1,l})}{B\log_2\left(1+\frac{\delta\left(\sum_{N_{1,l}=1}^{N_{1,l}}h_{N_{1,l},1,l}\right)^2}{\left(d_{l,N_{1,l}}d_{N_{1,l},FC}\right)^{\alpha}}\right)} + \ell\sum_{l=1}^{|G_2|+1}\left\|\mathbf{q}_{\pi_{2,l}} - \mathbf{q}_{\pi_{2,l-1}}\right\| + \\
&\sum_{l=1}^{|G_2|}\frac{\tilde{Q}(N_{2,l}\gamma_{2,l}+\zeta_{2,l})}{B\log_2\left(1+\frac{\delta\left(\sum_{N_{2,l}=1}^{N_{2,l}}h_{N_{2,l},2,l}\right)^2}{\left(d_{l,N_{2,l}}d_{N_{2,l},FC}\right)^{\alpha}}\right)} + \cdots + \ell\sum_{l=1}^{|G_M|+1}\left\|\mathbf{q}_{\pi_{M,l}} - \mathbf{q}_{\pi_{M,l-1}}\right\| + \sum_{l=1}^{|G_M|}\frac{\tilde{Q}(N_{M,l}\gamma_{M,l}+\zeta_{M,l})}{B\log_2\left(1+\frac{\delta\left(\sum_{N_{M,l}=1}^{N_{M,l}}h_{N_{M,l},M,l}\right)^2}{\left(d_{l,N_{M,l}}d_{N_{M,l},FC}\right)^{\alpha}}\right)}
\end{aligned}
\tag{23}
$$

Set $\left|g_{N_{m,l},FC}g_{l,N_{m,l}}\right| = \frac{h_{N_{m,l},m,l}}{\left(d_{l,N_{m,l}}d_{N_{m,l},FC}\right)^{\frac{\alpha}{2}}}$. By expanding Λ_{ω}, we can get (23), where $\ell = \frac{\omega_{wf}\psi_{cf}E_p^{mr}}{K\cdot\tilde{Q}} + \frac{1-\omega_{wf}}{V_{mr}}$.

Eq. (23) reveals that Λ_{ω} is composed of M sub-terms $\Lambda_{\omega,m}$. The objective of (P5) is to minimize Λ_{ω}, so we try to minimize each sub-term individually. Specifically, focusing on one sub-term $\Lambda_{\omega,m}$, which corresponds to the portion associated with UAV U_m in Λ_{ω}, we then analyze the minimization problem of $\Lambda_{\omega,m}$. The hovering point in (P5) is related to $\Lambda_{\omega,m}$, therefore $\Lambda_{\omega,m}$ can be expressed as a function of $\left\{\mathbf{q}_{\pi_{m,l}}\right\}$:

$$
\Lambda_{\omega,m}\left(\mathbf{q}_{\pi_{m,l}}\right) = \ell\sum_{l=1}^{|G_m|+1}\left\|\mathbf{q}_{\pi_{m,l}} - \mathbf{q}_{\pi_{m,l-1}}\right\| + \sum_{l=1}^{|G_m|}\frac{\tilde{Q}(N_{m,l}\gamma_{m,l}+\zeta_{m,l})}{B\log_2\left(1+\frac{\delta\left(\sum_{N_{m,l}=1}^{N_{m,l}}h_{N_{m,l},m,l}\right)^2}{\left(d_{l,N_{m,l}}d_{N_{m,l},FC}\right)^{\alpha}}\right)}
\tag{24}
$$

We consider using a convex optimization method to solve the hovering point $\left\{\mathbf{q}_{\pi_{m,l}}\right\}$. Since (11h) is non-convex, $d_{l,N_{m,l}}^2 d_{N_{m,l},FC}^2$ has been proven to be a non-convex function of $\left\{\mathbf{q}_{\pi_{m,l}}\right\}$ in our existing study [39]. We first introduce relaxation variables $u_{l,N_{m,l}}$ and $v_{N_{m,l},FC}$ that satisfy:

$$
u_{l,N_{m,l}}^{\alpha/2} \geq d_{l,N_{m,l}}^2
\tag{25}
$$

$$
v_{N_{m,l},FC}^{\alpha/2} \geq d_{N_{m,l},FC}^2
\tag{26}
$$

Then (24) can then be written as

$$\Lambda_{\omega,m}(\mathbf{q}_{\pi_{m,l}}) = \ell \sum_{l=1}^{|G_m|+1} \left\| \mathbf{q}_{\pi_{m,l}} - \mathbf{q}_{\pi_{m,l-1}} \right\| + \sum_{l=1}^{|G_m|} \frac{\tilde{Q}(N_{m,l}\gamma_{m,l} + \zeta_{m,l})}{B\log_2\left(1 + \frac{\delta\left(\sum_{N_{m,l}=1}^{N_{m,l}} h_{N_{m,l},m,l}\right)^2}{u_{l,N_{m,l}} v_{N_{m,l},FC}}\right)} \tag{27}$$

To obtain the optimal solution of UAV hovering position $\left\{\mathbf{q}_{\pi_{m,l}}\right\}$ at minimum $\Lambda_{\omega,m}(\mathbf{q}_{\pi_{m,l}})$, all the constraints in (25) and (26) must be satisfied with strict equality. We introduce the relaxation variable $\varsigma_{m,l}$ instead of $B\log_2\left(1 + \frac{\delta\left(\sum_{N_{m,l}=1}^{N_{m,l}} h_{N_{m,l},m,l}\right)^2}{u_{l,N_{m,l}} v_{N_{m,l},FC}}\right)$. The first-order Taylor of a convex function is a lower bound of its function at any point, let $u_{l,N_{m,l}}^{(j)}$ and $v_{N_{m,l},FC}^{(j)}$ be the j-th iteration of the given $u_{l,N_{m,l}}$ and $v_{N_{m,l},FC}$, respectively. The global lower bound of $B\log_2\left(1 + \frac{\delta\left(\sum_{N_{m,l}=1}^{N_{m,l}} h_{N_{m,l},m,l}\right)^2}{u_{l,N_{m,l}} v_{N_{m,l},FC}}\right)$ can be expressed as (28), where $\vartheta = \frac{B\delta\left(\sum_{N_{m,l}=1}^{N_{m,l}} h_{N_{m,l},m,l}\right)^2 \log_2^e}{u_{l,N_{m,l}}^{(j)} v_{N_{m,l},FC}^{(j)} + \delta\left(\sum_{N_{m,l}=1}^{N_{m,l}} h_{N_{m,l},m,l}\right)^2}$.

$$B\log_2\left(1 + \frac{\delta\left(\sum_{N_{m,l}=1}^{N_{m,l}} h_{N_{m,l},m,l}\right)^2}{u_{l,N_{m,l}} v_{N_{m,l},FC}}\right) \geq B\log_2\left(1 + \frac{\delta\left(\sum_{N_{m,l}=1}^{N_{m,l}} h_{N_{m,l},m,l}\right)^2}{u_{l,N_{m,l}}^{(j)} v_{N_{m,l},FC}^{(j)}}\right)$$
$$- \vartheta\left(\frac{u_{l,N_{m,l}} - u_{l,N_{m,l}}^{(j)}}{u_{l,N_{m,l}}^{(j)}} + \frac{v_{N_{m,l},FC} - v_{N_{m,l},FC}^{(j)}}{v_{N_{m,l},FC}^{(j)}}\right) \tag{28}$$

Based on the above analysis, we can formulate the minimization optimization problem of $\Lambda_{\omega,m}(\mathbf{q}_{\pi_{m,l}})$ as follows:

$$(\text{P6}): \min_{\left\{\mathbf{q}_{\pi_{m,l}}\right\}} \Lambda_{\omega,m} \tag{29a}$$

(11g)–(11i), (15c), (25)–(26) (29b)

$$\varsigma_{m,l} \leq B\log_2\left(1 + \frac{\delta\left(\sum_{N_{m,l}=1}^{N_{m,l}} h_{N_{m,l},m,l}\right)^2}{u_{l,N_{m,l}}^{(j)} v_{N_{m,l},FC}^{(j)}}\right) - \vartheta\left(\frac{u_{l,N_{m,l}} - u_{l,N_{m,l}}^{(j)}}{u_{l,N_{m,l}}^{(j)}} + \frac{v_{N_{m,l},FC} - v_{N_{m,l},FC}^{(j)}}{v_{N_{m,l},FC}^{(j)}}\right) \tag{29c}$$

After transformation, $\Lambda_{\omega,m}$ is a convex function, and its constraints are also convex functions, so (P6) is a linear convex optimization problem, which can be efficiently solved by the existing convex optimal toolbox such as CVX. See Algorithm 2 for details.

Algorithm 2: SCA-based algorithm for solving (P6)

1: Initialization: Given $\{\lambda_{m,k}\}$, $\{N_{m,l}\}$, and total iterations j_{total}. Initialize $\left\{\mathbf{q}_{\pi_{m,l}}^{(0)}\right\}$, the iteration number $j = 0$, and the convergence accuracy ε.
2: **repeat**
3: Solve the convex problem (P6) for given $\left\{\mathbf{q}_{\pi_{m,l}}^{(j)}\right\}$ and obtain the optimal solution as $\left\{\mathbf{q}_{\pi_{m,l}}^{*}\right\}$.
4: Update the point as $\mathbf{q}_{\pi_{m,l}}^{(j+1)} = \mathbf{q}_{\pi_{m,l}}^{*}$.
5: Update $j = j + 1$.
6: **until** The objective value $\Lambda_{\omega,m}$ converges within the prescribed accuracy ε.

In Algorithm 2, we typically initialize the hovering points at positions directly above the SNs, then iteratively solve for their optimal locations. Once the hovering points are determined, the UAV departs from its starting point, sequentially visits the hovering points within its associated SN group, and finally proceeds to the endpoint, thereby generating its flight trajectory. Although (P6) specifically analyzes the portion associated with the UAV U_m, this approach can be generalizable to multi-UAV scenarios. Algorithm 2 is applied to optimize all UAV hovering points of (P5).

According to (P6), the minimum value of $\Lambda_{\omega,m}$ depends on ℓ, $\gamma_{m,l}$ and $\zeta_{m,l}$, which are influenced by the weighting factor ω_{wf}. Therefore, selecting an appropriate value of ω_{wf} is essential.

Based on the comprehensive analysis above, we propose an alternating optimization algorithm to solve (P2). The detailed procedure is outlined in Algorithm 3.

Algorithm 3: SCA-based algorithm for solving (P2)

1: Initialization: Initialize the iteration number κ and the convergence accuracy ε.
2: for $i = 1 : \kappa$.
3: Solve (P3) with genetic algorithm to solve m-TSP problem to obtain SN-UAV association $\{\lambda_{m,k}\}$, and serving order $\{\pi_m\}$.
4: for $m = 1 : M$.
5: Using the CS-BJ algorithm to solve the optimal NoRE $\{N_{m,l}\}$ in (P4).
6: end
7: for $m = 1 : M$
8: for $j = 1 : j_{total}$
9: Using the SCA algorithm to solve the UAV hovering point $\left\{\mathbf{q}_{\pi_{m,l}}\right\}$ in (P5).
10: end
11: end
12: Based on (12) to calculate the updated $\Lambda_{\omega}^{(i+1)}$. If $\Lambda_{\omega}^{(i+1)} \leq \Lambda_{\omega}^{(i)}$. Update the SN-UAV association, the optimal NoRE, and the hovering point. Otherwise, break.
13: Update $i = i + 1$.
14: Until (P2) achieves the convergence accuracy ε or the number of iterations exceeds the value of κ.

In Algorithm 3, the genetic algorithm, CS-BJ algorithm, and SCA algorithm all converge to a certain extent. Additionally, a break condition is implemented: once the optimized Λ_{ω} increases, contradicting the optimization objective, Algorithm 2 halts variable updates and breaks, further ensuring convergence of Algorithm 2.

The overall complexity of Algorithm 3 is determined by the complexities of sub-problems (P3)–(P5). For (P3), genetic algorithm is used to solve the m-TSP problem, with its complexity roughly $O(M * K * \Delta)$, where Δ is the iteration number of genetic algorithm. For (P4), the CS-BJ algorithm is applied to solve the optimal NoRE used by each SN, with its complexity roughly $O(M * \log_2^K)$. For (P5), it is solved via SCA, its complexity is roughly $O((MK)^{3.5} \log_2^{1/\varepsilon})$, where ε is the accuracy of the SCA method for solving the problem. Thus, the total complexity of Algorithm 3 is approximately $O(\kappa(M * K * \Delta + M * \log_2^K + (MK)^{3.5} \log_2^{1/\varepsilon}))$, where κ denotes the number of iterations in Algorithm 3.

4 Numerical Results

4.1 Parameter Settings

In this section, the proposed optimization strategy is compared with the static collection benchmark, where the wake-up time allocation and NoRE are optimized using the genetic algorithm and Algorithm 1, respectively. We assume there are $K = 20$ SNs randomly distributed within a 500×500 m^2 area, with its center on the X-axis.

Four UAVs ($M = 4$) are deployed. The start and end of the UAVs flight trajectory at predefined coordinates $\mathbf{q}_I = [600, -250]$ (lower-left corner) and $\mathbf{q}_F = [100, 250]$ (upper-right corner) of the area. Given the negligible size of the IRS relative to transmission distances, the IRS coordinates are aligned with the UAV's position. The original hovering points of the UAVs are set directly above the sensors (static strategy). The UAV propulsion parameters follow Table 1 in [37]. The total system bandwidth $B = 2$ MHz is equally divided among the four UAVs. The FC is located at the origin $[x_d, y_d, 0] = [0, 0, 0]$. The EE's reciprocal (1/EE) is typically on the order of 10^{-5} Joules/bits for our considered system. The total mission completion time T_{total} is typically on the order of several hundred seconds. The compensation factor $\psi_{cf} = 10^7$ is therefore introduced to scale these two terms to a comparable numerical range, this enables the two variables to be of the same order of magnitude, ensuring that the weight ψ_{cf} can effectively and intuitively adjust the tradeoff between EE and total mission completion time. The main parameters used are shown in Table 1.

Table 1: Parameter setup

Parameters	Values
Noise power at the receiving end	$\sigma^2 = -100$ dbm
The FC's inherent power consumption of the circuit per time slot	$P_{d,k} = 10$ dbm [40]
The circuit's inherent power consumption of each SN	$P_{C,\pi_{m,l}} = 10$ dBm
The maximum energy budget per SN	$E_{\pi_{m,l},\max} = 1$ J
The transmit power of each SN	$p_k = 0.1$ W [41]
The efficiency of the power amplifier at transmitter (SN)	$\eta = 1.2$
The flight height of the UAVs	80 m [15]
The maximum power limit of the UAV	$P_{UAV,\max} = 100$W [33]
The NoRE of the IRS mounted on the UAV	50×50 [42]
The power consumption of each reflecting element in the IRS when provides the phase shift	$P_{IRS} = 5$ mW [43]
The MR speed of the UAV	$V_{mr} = 18.3$ m/s [44]

(Continued)

Table 1 (continued)

Parameters	Values
The maximum energy for each UAV	$E_{UAV,\max} = 3500$ J
The maximum speed of each UAV	$V_{max} = 30$ m/s
The path loss at the reference distance of 1 m	$\rho_0 = -30$ dB
The path loss exponent	$\alpha_t = 2.2$, $\alpha_r = 2.8$ [44]
The bandwidth	$B = 2$ MHz [7]
The compensation factor	$\psi_{cf} = 10^7$

4.2 Numerical Results

In this subsection, we first investigate the impact of varying transmission data amounts and weighting factors on the optimized trajectories and the required NoRE allocations. Subsequently, we evaluate how the weighting factor ω_{wf} influences the EE, total mission completion time, and Λ_w, with comparisons to the static collection benchmark.

Figs. 2 and 3 illustrate the optimized UAVs trajectories under varying transmission data amounts $\tilde{Q}$ (10 Mbits and 30 Mbits) and weighting factors ω_{wf} (0.3 and 0.7). By comparing Fig. 2a and b, as well as Fig. 3a and b, it can be observed that for identical weighting factor ω_{wf}, the optimized UAVs trajectories are closer to the SN when $\tilde{Q} = 30$ Mbits compared to $\tilde{Q} = 10$ Mbits. This occurs because a larger data amount requires a higher transmission rate to complete data transfer within the limited hovering time. Reducing the distance between the hovering point of the UAV and the SN shortens the propagation distance of the signal, improving the achievable rate. Although proximity to the SN increases the UAV's flight distance and raises the flight energy consumption, the significant gain in achievable rate outweighs the additional energy cost, reflecting a tradeoff between rate and power consumption.

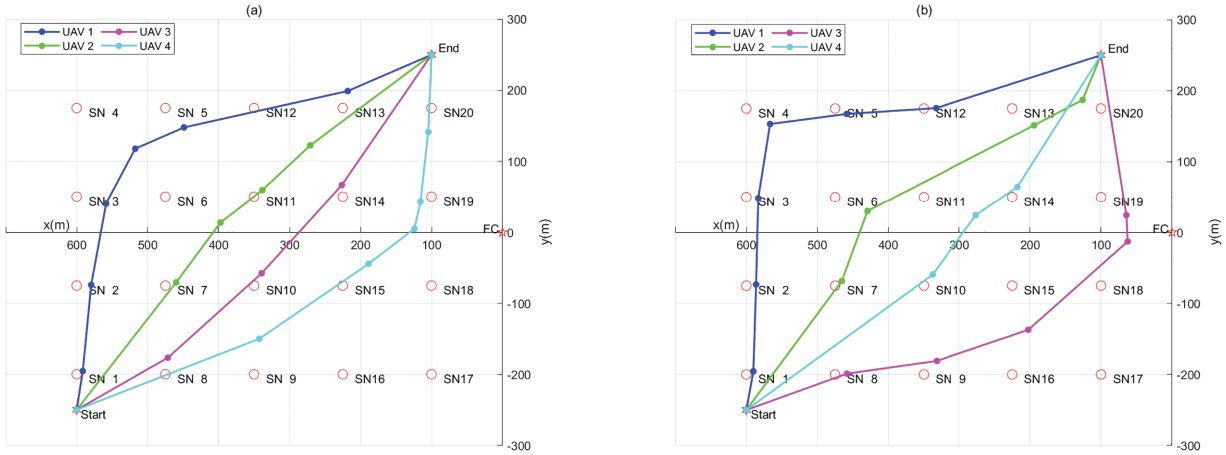

(a) $\tilde{Q} = 10Mbits$ **(b)** $\tilde{Q} = 30Mbits$

Figure 2: The optimized UAV trajectories with different data amounts $\tilde{Q}$ when the weighting factor $\omega_{wf} = 0.3$

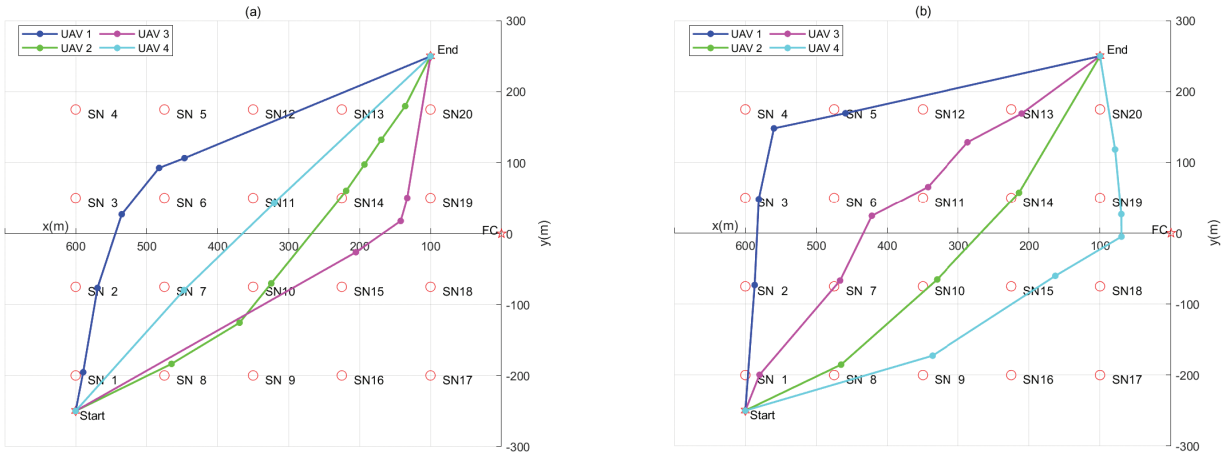

(a) $\tilde{Q} = 10Mbits$ **(b)** $\tilde{Q} = 30Mbits$

Figure 3: The optimized UAV trajectories with different data amounts $\tilde{Q}$ when the weighting factor $\omega_{wf} = 0.7$

For the same $\tilde{Q}$, distinct weighting factors ω_{wf} prioritize different optimization objectives: When $\omega_{wf} = 0.3$, it emphasizes minimizing the total mission completion time, whereas $\omega_{wf} = 0.7$ emphasizes maximizing EE. By comparing Figs. 2a and 3a, as well as Figs. 2b and 3b, for the same $\tilde{Q}$, distinct optimized trajectories emerge under different ω_{wf}. Notably, as ω_{wf} increases, the UAV's flight distance decreases, indicating that flight energy consumption is a critical factor affecting EE, which aligns with (6).

Fig. 4 illustrates the optimized NoREs under varying data transmission amounts $\tilde{Q}$ ($\tilde{Q}$ = 10 Mbits and $\tilde{Q}$ = 30 Mbits) and weighting factors ω_{wf} ($\omega_{wf} = 0.3$ and $\omega_{wf} = 0.7$). As shown in Fig. 4, for a given weighting factor ω_{wf}, the optimized NoRE at $\tilde{Q} = 30\,Mbits$ is significantly larger than that at $\tilde{Q} = 10\,Mbits$. This is because a higher data amount $\tilde{Q}$ demands more NoRE to satisfy data collection requirements, ensuring the data transmission is completed within the limited hovering time. Furthermore, by comparing the optimized NoRE for the same $\tilde{Q}$ under different weighting factors in Fig. 4a and b, the optimized NoRE under $\omega_{wf} = 0.3$ utilizes more NoRE than $\omega_{wf} = 0.7$. As proven in Proposition 1, the objective function of the optimization problem is a unimodal function of the NoRE. When $\omega_{wf} = 0.3$, the optimization is weighted toward minimizing the total task completion time. With more optimized NoRE, the achievable rate increases while the required hovering time decreases, which collectively contributes to reducing the overall mission completion time.

Figs. 5 and 6 compare the EE and total mission completion time of the proposed scheme against the static collection benchmark under varying data transmission volumes $\tilde{Q}$. The proposed solution achieves higher EE and shorter mission completion time compared to the benchmark across all $\tilde{Q}$, demonstrating its effectiveness.

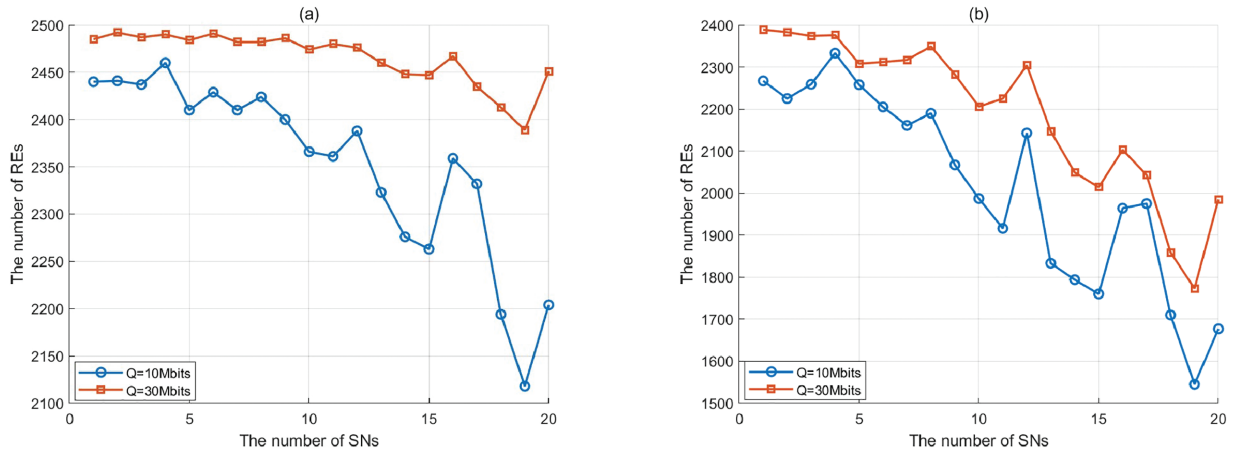

(a) $\omega_{wf} = 0.3$ **(b)** $\omega_{wf} = 0.7$

Figure 4: Optimized NoRE with different data amounts $\tilde{Q}$ and weighting factors ω_{wf}. ((**a**) ω_{wf} = 0.3, $\tilde{Q}$ = 10 Mbits and $\tilde{Q}$ = 30 Mbits. (**b**) ω_{wf} = 0.7, $\tilde{Q}$ = 10 Mbits and $\tilde{Q}$ = 30 Mbits.)

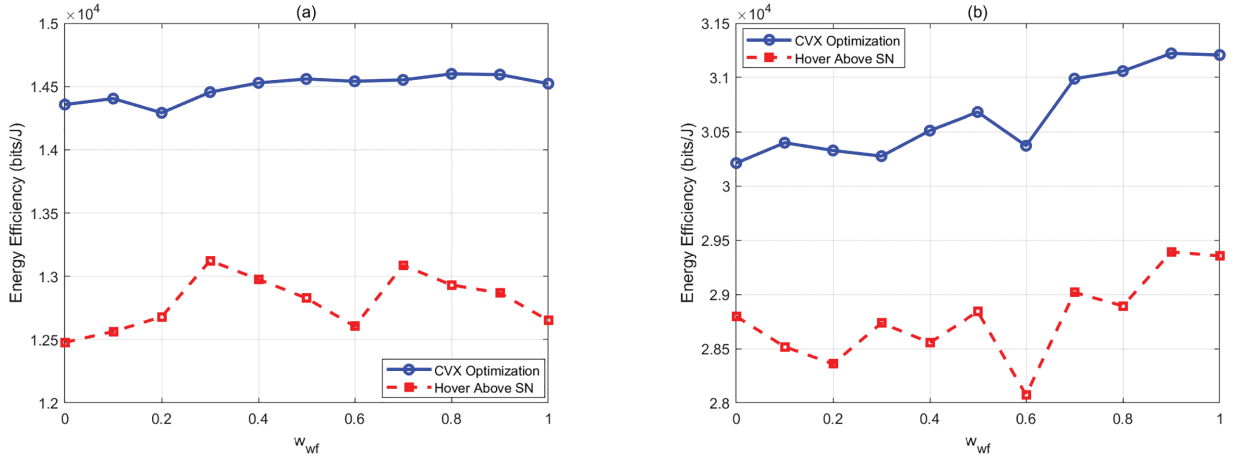

(a) $\tilde{Q} = 10Mbits$ **(b)** $\tilde{Q} = 30Mbits$

Figure 5: EE comparison of the two schemes with different $\tilde{Q}$

A larger $\tilde{Q}$ increases system EE but also extends mission completion time. That is to say, sacrificing time to get the gain of EE, necessitates a balance between EE gains and time costs. Of course, what we most expect is that simultaneously improve EE and reduce the total mission completion time, i.e., for $\tilde{Q}$ = 10 Mbits, select ω_{wf} = 0.4, and for $\tilde{Q}$ = 30 Mbits, select ω_{wf} = 0.7. Conversely, configurations that reduce EE while prolonging mission completion time should be avoided (e.g., ω_{wf} = 0.2 for $\tilde{Q}$ = 10 Mbits or ω_{wf} = 0.6 for $\tilde{Q}$ = 30 Mbits). When the transmitted data amount is 10 and 30 Mbits, compared to the static collection benchmark (the UAV hovers directly above each SN), the EE of the proposed method improves by more than 10.4% and 5.2%, while the total mission completion time is reduced by more than 5.4% and 3.3%, respectively.

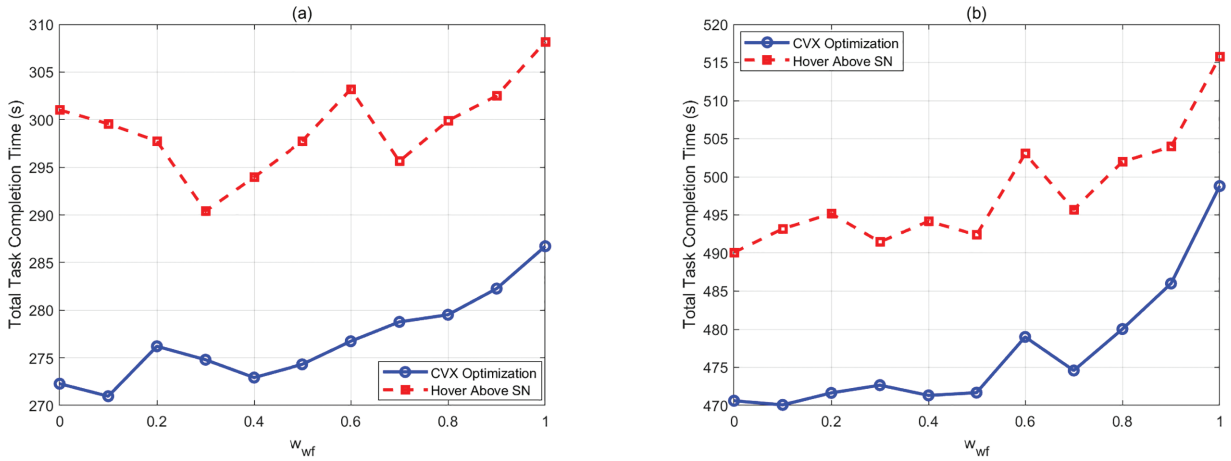

(a) $\tilde{Q} = 10Mbits$ **(b)** $\tilde{Q} = 30Mbits$

Figure 6: Total mission completion time comparison of the two schemes with different $\tilde{Q}$

Fig. 7 compares the weighted objective function Λ_w of the two schemes under varying data transmission amounts $\tilde{Q}$. The proposed solution achieves a smaller optimized Λ_w than the static collection benchmark across all $\tilde{Q}$, aligning with the goal of (P2), thereby validating the effectiveness of the proposed algorithm. In contrast, for $\tilde{Q}$ = 10 Mbits, Λ_w is minimized at $\omega_{wf} = 0$, indicating that minimizing the total mission completion time takes precedence over EE optimization in the objective function. For $\tilde{Q}$ = 30 Mbits, Λ_w is minimized at $\omega_{wf} = 1$, showing that EE optimization becomes more critical than reducing mission completion time. It implies for smaller data amounts, prioritizing shorter mission completion time reduces system costs, whereas for larger data amounts, prioritizing EE enhances system performance at the expense of longer mission time. This reflects an adaptive equilibrium between EE and mission completion time, embodying a compromise between system performance and operational cost.

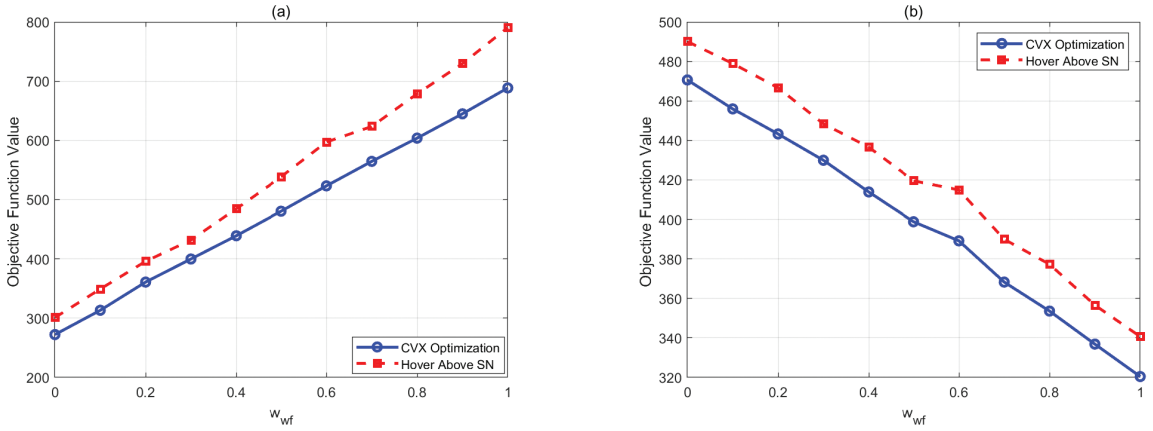

(a) $\tilde{Q} = 10Mbits$ **(b)** $\tilde{Q} = 30Mbits$

Figure 7: Comparison of Λ_w under the two schemes with different $\tilde{Q}$

5 Conclusion

This paper investigates the fundamental tradeoff between EE and the total mission completion time for data collection in multi-U-IRS-assisted IoT. We analyze the expressions of EE and total mission completion time. To ensure consistency in optimization objectives, we first formulate an optimization problem that minimizes the reciprocal of EE and the total mission completion time. Subsequently, we propose minimizing the weighted sum of the reciprocal of EE and the total mission completion time. Due to the intractability of directly solving the original problem, we decompose it into three subproblems and develop an alternating algorithm for optimization. Specifically, a genetic algorithm is employed to optimize UAV-SN association, the CS-BJ algorithm is used to optimize the NoRE, and the SCA is applied to optimize UAVs trajectories. Simulation results demonstrate that, compared to the static collection benchmark, the proposed solution achieves higher EE, shorter total mission completion time, and smaller objective function values under varying data amounts, highlighting its superiority and effectiveness. This work provides practical implications for UAV deployment in real IoT scenarios. For instance, in cost-sensitive, periodic agricultural monitoring, an operator can set a high ω_{wf} to prioritize EE, extending the fleet's operational lifetime and reducing long-term costs. Conversely, for time-sensitive tasks like post-disaster assessment, a low ω_{wf} can be used to generate mission plans that prioritize rapid data collection above all else.

For future research, it would be valuable to incorporate adaptive power control for the SNs, which could further enhance the EE and data rate of the system. In heterogeneous IoT applications, different SNs may exhibit significant variations in data generation rates due to their diverse monitoring task. Handling scenarios with heterogeneous data amounts represents a highly valuable research direction for the future, which will further enhance the universality of the proposed framework. A comprehensive empirical comparison between the proposed algorithm and a wider range of heuristic methods, including clustering and meta-heuristics, constitutes an important direction.

Acknowledgement: The authors would like to thank the Opening Project of Guangxi Wireless Broadband Communication and Signal Processing Key Laboratory, Key Laboratory of Cognitive Radio and Information Processing, Ministry of Education of China.

Funding Statement: This work was supported in part by the Opening Project of Guangxi Wireless Broadband Communication and Signal Processing Key Laboratory under Grant AD25069102; in part by the Basic Ability Improvement Project of Young and Middle Aged Teachers in Guangxi Universities, under Grant 2023KY0226; in part by Key Laboratory of Cognitive Radio and Information Processing, Ministry of Education of China, under Grant CRKL220108; in part by the Innovation Project of Guangxi Graduate Education, under Grant YCBZ2023131; in part by the Doctoral Research Foundation of Guilin University of Electronic Technology, under Grant UF23038Y; in part by the Bagui Youth Top Talent Project; in part by the Guangxi Key Research and Development Program under Grant AB25069510; in part by Open Fund of IPOC (BUPT), No. IPOC2024B07; in part by Guangxi Key Laboratory of Precision Navigation Technology and Application, under Grant DH202309.

Author Contributions: Hong Zhao: study conception and design, draft manuscript preparation; Hongbin Chen, Zhihui Guo: simulation setting, agricultural application scenario; Ling Zhan: analysis and interpretation of results; Shichao Li: paper discussion. All authors reviewed the results and approved the final version of the manuscript.

Availability of Data and Materials: No data and materials were used for the research described in the article.

Ethics Approval: Not applicable.

Conflicts of Interest: The authors declare no conflicts of interest to report regarding the present study.

Appendix A

We first analyze the variation of $F(N_{m,l})$ under the condition $1 \le N_{m,l} \le N$. As $N_{m,l}$ increases, $F(N_{m,l})$ exhibits the following trends:

1) $F(N_{m,l})$ monotonically decreases with increasing $N_{m,l}$.

2) There always exists an optimized NoRE $\tilde{N}_{m,l}$ such that $F(\tilde{N}_{m,l}) \le F(\tilde{N}_{m,l}+1) \le F(\tilde{N}_{m,l}+2) \le \cdots$.

When $F(\tilde{N}_{m,l}) \le F(\tilde{N}_{m,l}+1)$, we derive:

$$\frac{\tilde{Q}}{B\log_2\left(1+\delta\left(\sum\limits_{\tilde{N}_{m,l}=1}^{N}\beta_{\tilde{N}_{m,l}}\right)^2\right)}(\tilde{N}_{m,l}\gamma_{m,l}+\zeta_{m,l}) = \frac{\tilde{Q}(\tilde{N}_{m,l}\gamma_{m,l}+\zeta_{m,l})}{R_{\pi_{m,l}}(N_{m,l})} \le \frac{\tilde{Q}((\tilde{N}_{m,l}+1)\gamma_{m,l}+\zeta_{m,l})}{R_{\pi_{m,l}}(N_{m,l}+1)} \tag{A1}$$

Expanding both sides of inequality (A1) yields:

$$\begin{aligned}\tilde{N}_{m,l} &\le -\frac{\zeta_{m,l}}{\gamma_{m,l}} + \frac{R_{\pi_{m,l}}(N_{m,l})}{R_{\pi_{m,l}}(N_{m,l}+1)-R_{\pi_{m,l}}(N_{m,l})} \\ &= -\frac{\zeta_{m,l}}{\gamma_{m,l}} + \frac{-(R_{\pi_{m,l}}(N_{m,l}+1)-R_{\pi_{m,l}}(N_{m,l}))+R_{\pi_{m,l}}(N_{m,l}+1)}{R_{\pi_{m,l}}(N_{m,l}+1)-R_{\pi_{m,l}}(N_{m,l})} \\ &= -\frac{\zeta_{m,l}}{\gamma_{m,l}} - 1 + \frac{R_{\pi_{m,l}}(N_{m,l}+1)}{R_{\pi_{m,l}}(N_{m,l}+1)-R_{\pi_{m,l}}(N_{m,l})}\end{aligned} \tag{A2}$$

Since $R_{\pi_{m,l}}(N_{m,l}+1)-R_{\pi_{m,l}}(N_{m,l}) \ge R_{\pi_{m,l}}(N_{m,l}+2)-R_{\pi_{m,l}}(N_{m,l}+1)$, inequality (A2) can be rewritten as:

$$\tilde{N}_{m,l} \le -\frac{\zeta_{m,l}}{\gamma_{m,l}} - 1 + \frac{R_{\pi_{m,l}}(N_{m,l}+1)}{R_{\pi_{m,l}}(N_{m,l}+1)-R_{\pi_{m,l}}(N_{m,l})} \le -\frac{\zeta_{m,l}}{\gamma_{m,l}} - 1 + \frac{R_{\pi_{m,l}}(N_{m,l}+1)}{R_{\pi_{m,l}}(N_{m,l}+2)-R_{\pi_{m,l}}(N_{m,l}+1)} \tag{A3}$$

Based on inequality (A3), we further obtain $F(\tilde{N}_{m,l}+1) \le F(\tilde{N}_{m,l}+2)$. By extension, $F(\tilde{N}_{m,l}) \le F(\tilde{N}_{m,l}+1) \le F(\tilde{N}_{m,l}+2) \le \cdots$ can be derived.

The above analysis proves that $F(N_{m,l})$ is a unimodal function when $1 \le N_{m,l} \le N$. In (P4), the numerical range of $N_{m,l}$ can be determined using constraints (11e), (11g)–(11i), thereby revealing the trend of $F(N_{m,l})$ within this range.

References

1. Nguyen K-V, Nguyen C-H, Do TV, Rotter C. Efficient multi-UAV assisted data gathering schemes for maximizing the operation time of wireless sensor networks in precision farming. IEEE Trans Ind Informat. 2023;19(12):11664–74. doi:10.1109/tii.2023.3248616.
2. Jiao L, Gao L, Zheng J, Yang P, Xue W. Resource allocation in RISs-assisted UAV-enabled MEC network with computation capacity improvement. Comput Commun. 2024;228:107953. doi:10.1016/j.comcom.2024.107953.
3. Huo X, Zhang H, Wang Z, Huang C, Yan H. Energy minimization for UAV-enabled data collection with guaranteed performance. IEEE Trans Veh Technol. 2024;73(12):19613–24. doi:10.1109/tvt.2024.3449639.
4. Bakirci M. A novel swarm unmanned aerial vehicle system: incorporating autonomous flight, real-time object detection, and coordinated intelligence for enhanced performance. Trait Signal. 2023;40(5):2063–78. doi:10.18280/ts.400524.
5. Kim C, Choi HH, Lee K. Joint optimization of trajectory and resource allocation for multi-UAV-enabled wireless-powered communication networks. IEEE Trans Commun. 2024;72(9):5752–64. doi:10.1109/tcomm.2024.3383113.

6. Kang M, Jeon S-W. Energy-efficient data aggregation and collection for multi-UAV-enabled IoT networks. IEEE Wireless Commun Lett. 2024;13(4):1004–8. doi:10.1109/lwc.2024.3355934.
7. Li M, He S, Li H. Minimizing mission completion time of UAVs by jointly optimizing the flight and data collection trajectory in UAV-enabled WSNs. IEEE Internet Things J. 2022;9(15):13498–510. doi:10.1109/jiot.2022.3142764.
8. Zhan C, Zeng Y. Aerial-ground cost tradeoff for multi-UAV-enabled data collection in wireless sensor networks. IEEE Trans Commun. 2020;68(3):1937–50. doi:10.1109/tcomm.2019.2962479.
9. Zhang H, Tao Y, Lv X, Liu Y. Leader follower UAV-assisted WSNs for improving data collection rate and shortening flight time. IEEE Sens J. 2023;23:26597–607. doi:10.1109/jsen.2023.3312733.
10. Xu Y, Zhang T, Liu Y, Yang D, Xiao L, Tao M. 3D multi-UAV computing networks: computation capacity and energy consumption tradeoff. IEEE Trans Veh Technol. 2024;73:10627–41. doi:10.1109/tvt.2024.3372292.
11. Jia R, Fu Q, Zheng Z, Zhang G, Li M. Energy and time trade-off optimization for multi-UAV enabled data collection of IoT devices. IEEE/ACM Trans Netw. 2024;32(6):5172–87. doi:10.1109/tnet.2024.3450489.
12. Yuan X, Hu S, Ni W, Wang X, Jamalipour A. Deep reinforcement learning-driven reconfigurable intelligent surface-assisted radio surveillance with a fixed-wing UAV. IEEE Trans Inf Forensics Secur. 2023;18:4546–60. doi:10.1109/tifs.2023.3297021.
13. Chen L, Wang Z. Multi-UAV trajectory planning for RIS-assisted SWIPT system under connectivity preservation. Comput Netw. 2024;255:110906. doi:10.1016/j.comnet.2024.110906.
14. Zhang Q, Saad W, Bennis M. Reflections in the sky: millimeter wave communication with UAV-carried intelligent reflectors. In: 2019 IEEE Global Communications Conference (GLOBECOM); 2019 Dec 9–13; Waikoloa, HI, USA. p. 1–6.
15. Nguyen-Kha H, Nguyen HV, Le MTP, Shin OS. Joint UAV placement and IRS phase shift optimization in downlink networks. IEEE Access. 2022;10:111221–31. doi:10.1109/access.2022.3214663.
16. You C, Kang Z, Zeng Y, Zhang R. Enabling smart reflection in integrated air-ground wireless network: IRS meets UAV. IEEE Wireless Commun. 2021;28(6):138–44. doi:10.1109/mwc.001.2100148.
17. Peng Y, Tang J, Yang Q, Han Z, Ma J. Joint power allocation algorithm for UAV-borne simultaneous transmitting and reflecting reconfigurable intelligent surface-assisted non-orthogonal multiple access system. IEEE Access. 2023;11:140506–18. doi:10.1109/access.2023.3342049.
18. Liu Y, Han F, Zhao S. Flexible and reliable multiuser SWIPT IoT network enhanced by UAV-mounted intelligent reflecting surface. IEEE Trans Rel. 2022;71(2):1092–103. doi:10.1109/tr.2022.3161336.
19. Adam ABM, Ouamri MA, Wan X, Muthanna MSA, Alkanhel R, Muthanna A, et al. Secure communication in UAV–RIS-empowered multiuser networks: joint beamforming, phase shift, and UAV trajectory optimization. IEEE Syst J. 2024;18(2):1009–19. doi:10.1109/jsyst.2024.3379456.
20. Dang X-T, Nguyen HV, Shin O-S. Physical layer security for IRS-UAV-assisted cell-free massive MIMO systems. IEEE Access. 2024;12:89520–37. doi:10.1109/access.2024.3419888.
21. Nnamani CO, Khandaker MR, Sellathurai M. Secure data collection via UAV-carried IRS. ICT Express. 2023;9(4):706–13. doi:10.1016/j.icte.2022.09.003.
22. Tyrovolas D, Mitsiou NA, Boufikos TG, Mekikis P-V, Tegos SA, Diamantoulakis PD, et al. Energy-aware trajectory optimization for UAV-mounted RIS and full-duplex relay. IEEE Internet Things J. 2024;11(13):24259–72. doi:10.1109/jiot.2024.3390767.
23. Tyrovolas D, Mekikis P-V, Tegos SA, Diamantoulakis PD, Liaskos CK, Karagiannidis GK. Energy-aware design of UAV-mounted RIS networks for IoT data collection. IEEE Trans Commun. 2023;71(2):1168–78. doi:10.1109/tcomm.2022.3229672.
24. Mohamed EM, Hashima S, Hatano K. Energy aware multi-armed bandit for millimeter wave-based UAV mounted RIS networks. IEEE Wireless Commun Lett. 2022;11(6):1293–7. doi:10.1109/lwc.2022.3164939.
25. Zeng Y, Zhang R. Energy-efficient UAV communication with trajectory optimization. IEEE Trans Wireless Commun. 2017;16(6):3747–60. doi:10.1109/twc.2017.2688328.
26. Xiao Y, Tyrovolas D, Tegos SA, Diamantoulakis PD, Ma Z, Hao L, et al. Solar powered UAV-mounted RIS networks. IEEE Commun Lett. 2023;27(6):1565–9. doi:10.1109/lcomm.2023.3264493.

27. Yang H, Lin K, Xiao L, Zhao Y, Xiong Z, Han Z. Energy harvesting UAV-RIS-assisted maritime communications based on deep reinforcement learning against jamming. IEEE Trans Wireless Commun. 2024;23(8):9854–68. doi:10.1109/twc.2024.3367034.
28. Mamaghani MT, Hong Y. Aerial intelligent reflecting surface-enabled Terahertz covert communications in beyond-5G Internet of Things. IEEE Internet Things J. 2022;9(19):19012–33. doi:10.1109/jiot.2022.3163396.
29. Ge L, Zhang H, Wang J-B, Li GY. Reconfigurable wireless relaying with multi-UAV-carried intelligent reflecting surfaces. IEEE Trans Veh Technol. 2023;72(4):4932–47. doi:10.1109/tvt.2022.3227623.
30. Liao Y, Song Y, Xia S, Han Y, Xu N, Zhai X. Energy minimization of RIS-assisted cooperative UAV-USV MEC network. IEEE Internet Things J. 2024;11(20):32490–502. doi:10.1109/jiot.2024.3432151.
31. Van Vinh N. Performance enhancement of nonorthogonal multiple access systems by multiple UAVs and RISs. Digit Signal Process. 2023;140:104136. doi:10.1016/j.dsp.2023.104136.
32. Sun S, Zhang G, Mei H, Wang K, Yang K. Optimizing multi-UAV deployment in 3-D space to minimize task completion time in UAV-enabled mobile edge computing systems. IEEE Commun Lett. 2020;25(2):579–83. doi:10.1109/lcomm.2020.3029144.
33. Zeng Y, Xu J, Zhang R. Energy minimization for wireless communication with rotary-wing UAV. IEEE Trans Wireless Commun. 2019;18(4):2329–45. doi:10.1109/twc.2019.2902559.
34. Shen S, Yang K, Wang K, Zhang G, Mei H. Number and operation time minimization for multi-UAV-enabled data collection system with time windows. IEEE Internet Things J. 2022;9(12):10149–61. doi:10.1109/jiot.2021.3121511.
35. Zhan C, Zeng Y. Completion time minimization for multi-UAV-enabled data collection. IEEE Trans Wireless Commun. 2019;18(10):4859–72. doi:10.1109/twc.2019.2930190.
36. Shang B, Shafin R, Liu L. UAV swarm-enabled aerial reconfigurable intelligent surface: modeling, analysis, and optimization. IEEE Trans Commun. 2023;71(6):3621–36. doi:10.1109/tcomm.2022.3173369.
37. Mustaghfirin M, Singh K, Biswas S, Huang W-J. Performance analysis of intelligent reflecting surface-assisted multi-users communication networks. Electronics. 2021;10(17):2084. doi:10.3390/electronics10172084.
38. Zhao H, Chen H, Tan F, Zhan L. Optimum number of reflecting elements for UAV mounted intelligent reflecting surface-assisted data collection in wireless sensor network. IEEE Sens J. 2024;24(14):23062–74. doi:10.1109/jsen.2024.3407771.
39. Zhao H, Chen H, Li S, Zhan L. Joint Optimization of UAV trajectory and number of reflecting elements for UAV-mounted intelligent reflecting surface-assisted data collection in wireless sensor networks under transmission prioritized scheme. IEEE Trans Green Commun Netw. 2021;10:276–80. doi:10.1109/lwc.2020.3027969.
40. Li D. How many reflecting elements are needed for energy- and spectral-efficient intelligent reflecting surface-assisted communication. IEEE Trans Commun. 2022;70(2):1320–31. doi:10.1109/tcomm.2021.3128544.
41. Zhan C, Zeng Y, Zhang R. Energy-efficient data collection in UAV enabled wireless sensor network. IEEE Wirel Commun Lett. 2018;7(3):328–31. doi:10.1109/lwc.2017.2776922.
42. Tang W, Li X, Dai JY, Jin S, Zeng Y, Cheng Q, et al. Wireless communications with programmable metasurface: transceiver design and experimental results. China Commun. 2019;16(5):46–61. doi:10.23919/j.cc.2019.05.004.
43. Nguyen NT, Vu Q-D, Lee K, Juntti M. Hybrid relay-reflecting intelligent surface-assisted wireless communications. IEEE Trans Veh Technol. 2022;71(6):6228–44. doi:10.1109/tvt.2022.3158686.
44. Ren H, Zhang Z, Peng Z, Li L, Pan C. Energy minimization in RIS-assisted UAV-enabled wireless power transfer systems. IEEE Internet Things J. 2023;10(7):5794–809. doi:10.1109/jiot.2022.3150178.